Dalton Transactions

ROYAL SOCIETY OF CHEMISTRY

PAPER

View Article Online
View Journal | View Issue

Cite this: *Dalton Trans.*, 2026, **55**, 7709

Structural diversity of dimethylgallium naphthalene-2,3-dicarboxylate/pyridine systems

Maksymilian Solka,†[a] Michał Terlecki,†[b] Iwona Justyniak,*[a] Wanda Ziemkowska,[b] Daniel Prochowicz[a] and Janusz Lewiński*[a,b]

Group 13 organometallic complexes are versatile building blocks of supramolecular architectures, offering wide structural and functional diversity. While organoaluminum systems have been extensively explored as nodes or chiral metalloligands in the construction of coordination frameworks, their heavier congeners remain far less investigated. Herein, we examined the reactivity of a new macrocyclic organogallium derivative of 2,3-naphthalenedicarboxylic acid (*naphtha*-H_2), $[(Me_2Ga)_2(naphtha)]_2$ (**1**), toward selected mono- and bifunctional pyridine Lewis bases, as well as the chiral metalloligand $[Me_2Al(CN)]_2$ (where CN = deprotonated cinchonine). The results show that, in the presence of neutral Lewis bases, the macrocyclic structure of the parent complex **1** undergoes cleavage accompanied by rearrangement into various four-coordinate pyridine adducts, which, in the case of 4,4′-bipyridine (*bipy*), leads to the formation of a new 1D coordination polymer $[(Me_2Ga)_2(naphtha)(bipy)]_n$. Moreover, we show that the reaction of **1** with the chiral organoaluminum *N*,*N*′-ditopic metalloligand $[Me_2Al(CN)]_2$ proceeds *via* an intriguing transalkylation pathway, affording an original complex $[(MeAl)_2(naphtha)(CN)_2(GaMe_3)_2]$. Together with our previous studies on the organoaluminum analogue of **1**, this work provides new insight into how the nature of the Group 13 metal center governs Lewis acidity of organometallic complexes and their reactivity toward *N*,*N*′-ditopic linkers.

Received 11th February 2026,
Accepted 10th April 2026

DOI: 10.1039/d6dt00374e

rsc.li/dalton

Introduction

Coordination polymers are structurally well-defined materials constructed from inorganic nodes and organic linkers, enabling control over the topology and functionality of extended frameworks.[1–5] Group 13 metal centres, particularly aluminium-based nodes, are widely employed in metal–organic frameworks (MOFs) with diverse applications.[6–10] Recent studies have highlighted the key role of Lewis acidity and coordination preferences of Group 13 centres in directing the formation and dimensionality of coordination polymers. In particular, systems based on aluminium and gallium halides or organometallic derivatives linked by N-donor ligands have demonstrated that subtle differences in metal–ligand interactions may lead to markedly different structural outcomes, ranging from discrete adducts to extended polymeric networks.[6,11,12] Such observations underscore the importance of controlling both the intrinsic Lewis acidity of the metal centre and the topology of the linker in order to achieve predictable framework assembly.

Despite extensive studies, the reactivity of octet-compliant, four-coordinate Group 13 complexes toward donor ligands remains insufficiently understood.[13,14] In particular, it is unclear which factors determine whether such species form simple adducts or undergo deeper structural reorganization, limiting their rational use in framework design.[6,11,15–17] Heteroleptic Group 13 organometallics are especially attractive in this context, as their structures can be tuned through both the ligand framework and the identity of the metal center. Consequently, they represent particularly attractive building units that offer substantial diversity in supramolecular architectures, arising from the ligands identity and both the coordination geometry and the nature of the metal center. These features enable the construction of non-covalent interactions-directed assemblies,[18] macrocyclic networks,[19–22] and coordination polymers, where Group 13 organometallics act as nodes[16,22,23] or chiral metalloligands.[24] Nevertheless, comparative studies addressing how the identity of the metal centre (*e.g.*, Al *vs.* Ga) governs these processes are scarce. In this context, our work focuses on elucidating the relationship between metal-dependent Lewis acidity, ligand topology, and structural outcome in coordination-driven assembly. In particular, we address whether the reduced tendency of gallium to

[a]*Institute of Physical Chemistry, Polish Academy of Sciences, Kasprzaka 44/52, 01-224 Warsaw, Poland. E-mail: janusz.lewinski@pw.edu.pl, ijustyniak@ichf.edu.pl*
[b]*Faculty of Chemistry, Warsaw University of Technology, Noakowskiego 3, 00-664 Warsaw, Poland*
†These authors contributed equally to this work.

adopt higher coordination numbers alters the balance between framework formation and structural reorganization.

Carboxylate-stabilized Group 13 organometallic derivatives, in particular, provide a convenient platform for probing structure–reactivity–property relationships.[13,16,22,25–29] In our previous studies, we showed that four-coordinate Group 13 carboxylates can form stable five-coordinate adducts with neutral Lewis bases, a phenomenon termed "dormant" Lewis acidity (Fig. 1a).[29] More recently, we extended this concept to a tetranuclear organoaluminum derivative of 2,3-naphthalenedicarboxylic acid (*naphtha*-H_2), which acts as a dormant poly-Lewis acid and, in combination with the rigid *N*,*N*′-ditopic Lewis base 1,2-bis(4-pyridyl)ethylene (*bpee*), serves as a node for the formation of the 1D coordination polymer $[\{(Me_2Al)_2(naphtha)\}_2(bpee)]_n$ (Fig. 1b).[16] Notably, reactions of organoaluminum complexes with neutral Lewis bases may yield markedly different outcomes, ranging from simple Lewis acid–base adducts that preserve the parent cluster structure (Fig. 2b and d) to complete structural rearrangements (Fig. 2c). Notably, factors governing these divergent reactivity pathways remain poorly understood.

While organoaluminum systems have been extensively investigated, their heavier congeners remain significantly less explored.[18,23,30,31] Herein, motivated by our interest in how the nature of the metal center in Group 13 organometallic complexes governs their Lewis acidity and reactivity toward various *N*,*N*′-ditopic linkers, we employ a new *naphtha*-stabilized organogallium complex $[(Me_2Ga)_2(naphtha)]_2$ (**1**) as a model Ga-based poly-Lewis acid that is isostructural with the previously studied organoaluminum analogue (Fig. 2a). We examined its reactivity toward selected mono- and bifunctional Lewis bases, including 4-methylpyridine, bipyridines with different organic backbones, as well as a chiral *N*,*N*′-ditopic organoaluminium metaloligand, highlighting distinct differences in the reactivity of organometallic Ga- and Al-based systems (Fig. 2b–j).

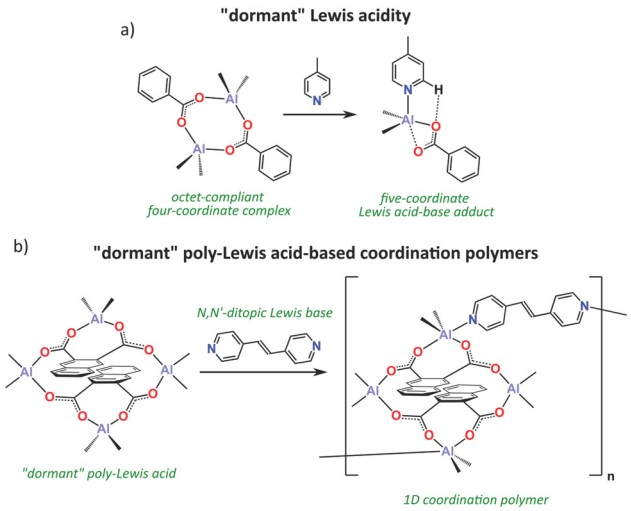

Fig. 1 Concept of "dormant" Lewis acidity (a) and its utilization for construction of coordination polymers (b).

Results and discussion

Previously, we showed that the tetranuclear organoaluminum complex $[(Me_2Al)_2(naphtha)]_2$ can act as a dormant poly-Lewis

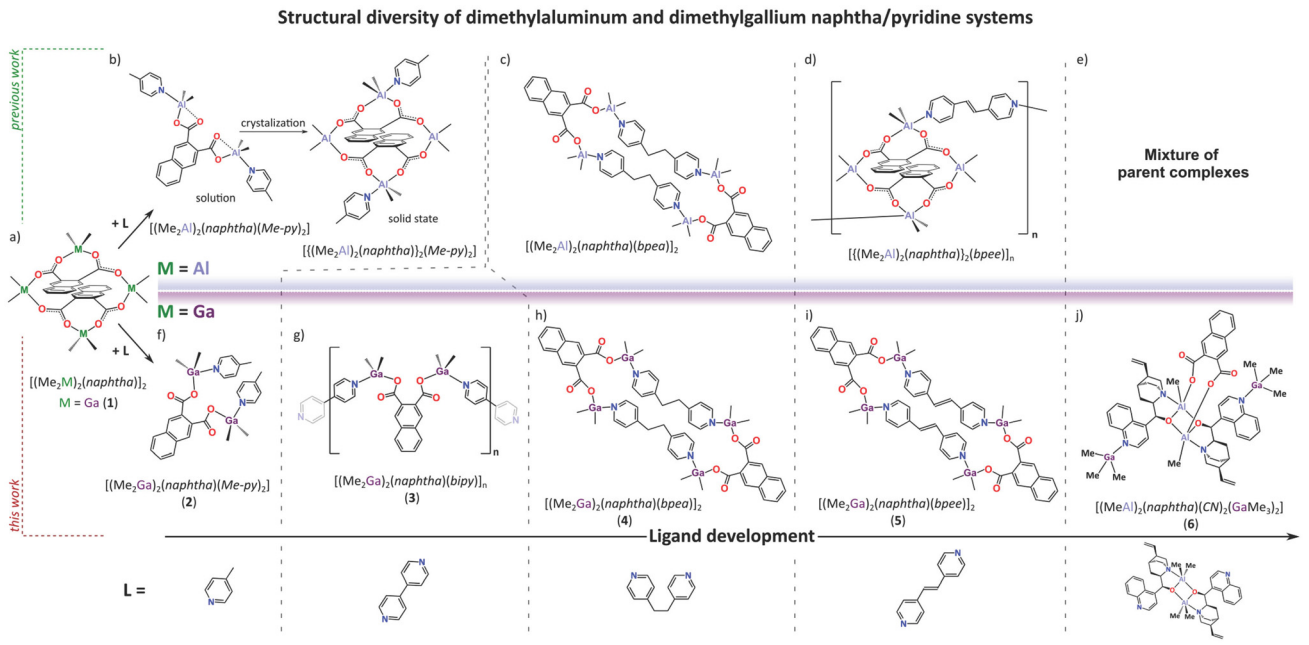

Fig. 2 Reactivity of $[(Me_2Al)_2(naphtha)]_2$ and $[(Me_2Ga)_2(naphtha)]_2$ (a) toward *Me-py* (b and f), various *N*,*N*′-ditopic linkers (c–d, g–i), as well as chiral organoaluminum metalloligand $[Me_2Al(CN)]_2$ (e and j).

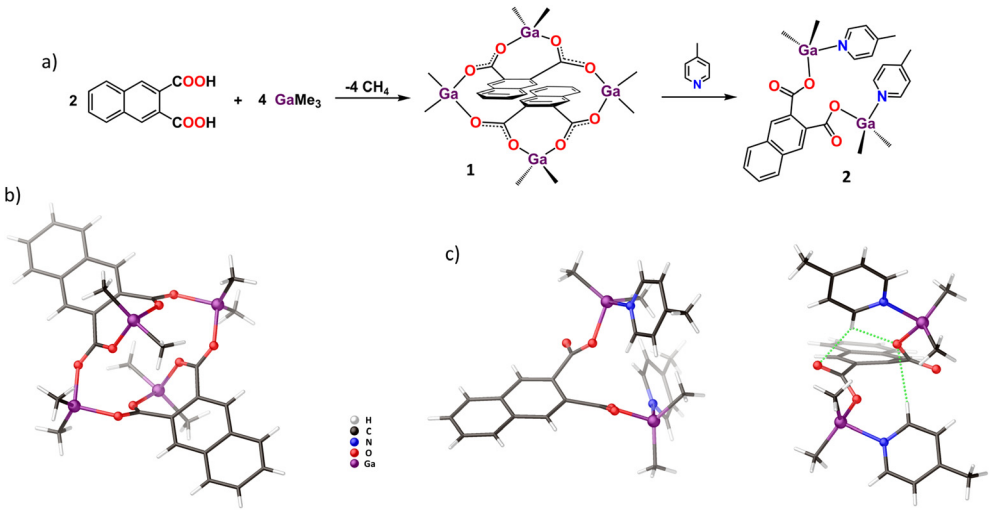

Fig. 3 Schematic representation of the synthesis of organogallium complex **1** and its reactivity toward *Me-py* (a) and molecular structure of complex **1** (b) and **2** (two views) (c).

acid, exhibiting versatile reactivity toward neutral mono- and ditopic Lewis bases, with either preservation or cleavage of the parent macrocycle structure depending on the character of donor pyridine ligands (Fig. 2a–d).[16] In order to determine how the nature of the metal center affects the chemical properties of such systems, we synthesized the isostructural organogallium complex $[(Me_2Ga)_2(naphtha)]_2$ (**1**) and probed its reactivity toward 4-methylpyridine, bipyridines with different organic backbones, as well as the chiral metalloligand $[Me_2Al(CN)]_2$ (where CN = deprotonated cinchonine)[24] (Fig. 2a and f–j). The resulting Lewis acid–base adducts were characterized in solid-state by single-crystal X-ray diffraction (SCXRD), Fourier transform infrared spectroscopy (FTIR), and elemental analysis, and, in the case of soluble products, also by solution ^{1}H and ^{13}C NMR spectroscopy.

Synthesis and characterization of tetranuclear gallium aggregate 1 and its reactivity toward monodentate neutral Lewis base

A new tetranuclear organogallium complex **1** was synthesized by the reaction of *naphtha*-H_2 with 2 equiv. of $GaMe_3$ in a dichloromethane (DCM) solution (Fig. 3a). Well-defined crystals of **1** were isolated in high yield (85%) by crystallization from concentrated post-reaction mixture at 5 °C. The ^{1}H NMR spectrum of **1** in $CDCl_3$ shows three aromatic multiplets attributed to the *naphtha* ligand at 8.43, 8.00, and 7.68 ppm, as well as three singlets at −0.03, −0.66, and −0.84 ppm corresponding to three inequivalent Ga–Me environments, one associated with the bridging Me_2Al units and two with the chelated Me_2Al moieties (Fig. S8), which is consistent with the solid-state structure determined by SCXRD (*vide infra*). Accordingly, the ^{13}C NMR spectrum, besides resonances from the *naphtha* ligand at 177.6 and 133.7–128.9 ppm, displays three signals form Ga–Me groups at −5.8, −7.6, −8.1 ppm. The solid state FTIR spectrum of **1** shows two $\nu_{asym}(CO_2)$ bands at 1589 and 1537 cm^{-1} and one $\nu_{sym}(CO_2)$ band at 1415 cm^{-1} (Fig. S11), indicating a carboxylate coordination mode similar to that observed in the previously reported complex $[(Me_2Al)_2(naphtha)]_2$,[16] that is a μ_3–κ^2:η^1:η^1 mode. SCXRD analysis confirms that the molecular structure of **1** is isostructural to its aluminum analogue; however, the two compounds display different unit cell parameters, arising from variations in crystal packing. Particularly, whereas $[(Me_2Al)_2(naphtha)]_2$ was isolated from a toluene solution as an unsolvated phase, the gallium complex **1** crystallizes from DCM solution as a **1**·0.5DCM solvate, which affects the arrangement of molecules in the crystal lattice.

Compound **1** is isostructural with other dimethylaluminium and dimethylgallium complexes stabilized by *ortho*-dicarboxylate ligands;[16,23] for other examples of macrocyclic alkylgallium carboxylates, see: ref. 32–36. The molecular structure of **1** comprises three fused heterocyclic rings – one 16-membered and two 7-membered – and features two types of differently coordinated Me_2Ga units (Fig. 3b). Each *naphtha* ligand in **1** chelates one Me_2Ga unit between both carboxylate groups, forming 7-membered $\{GaOC_4O\}$ rings. The resulting $[Me_2Ga(\kappa_2\text{-}naphtha)]$ moieties are further bridged by two additional Me_2Ga units to form a central 16-membered $\{GaOCOGaOCO\}_2$ macrocycle. Both types of Ga centers adopt distorted tetrahedral coordination geometries, with the deviation from ideal T_d geometry being slightly greater for the chelated Ga sites than for the bridging ones (see, continuous shape measures (CShM) analysis in SI). The carboxylate groups adopt a μ_3–κ^2:η^1:η^1 coordination mode with *syn–anti* conformation with respect to the Ga centers.

Having established the structure of **1**, we next examined its dormant poly-Lewis acid reactivity toward 4-methylpyridine (*Me-py*) as a model monodentate Lewis base. The addition of 4 equiv. of *Me-py* to a DCM solution of **1** afforded a Lewis-acid–base adduct $[\{Me_2Ga(Me\text{-}py)\}_2(naphtha)]$ (**2**) (Fig. 3a). High-

quality crystals of **2** were isolated in high yield (67%) by crystallization from the concentrated parent solution at 5 °C. The ^{1}H NMR spectrum of **2** in $CDCl_3$ displays five aromatic resonances in the 7.2–8.5 ppm range arising from *naphtha* and *Me-py* ligands, a singlet at 2.37 ppm corresponding to the *Me-py* methyl group, and a single resonance at −0.21 ppm associated with equivalent Me–Ga groups (Fig. S9). The respective intensity of signals confirms the coordination of one *Me-py* molecule per Me_2Ga unit. The ^{13}C NMR spectrum shows set of signals at 174.3 and 151.7–126.1 ppm attributed to the *naphtha* ligand and aromatic carbon atoms of *Me-py*, resonance at 21.5 ppm from *Me-py* methyl group, and single resonance at −6.5 ppm associated with the presence of equivalent Me–Ga groups. In the solid-state FTIR spectrum, complex **2** exhibits $\nu_{asym}(CO_2)$ bands at 1640 and 1621 cm^{-1} and $\nu_{sym}(CO_2)$ band at 1328 cm^{-1} (Fig. S11). The pronounced blue shift of the $\nu_{asym}(CO_2)$ bands relative to **1**, together with the increased $\Delta\nu$ between $\nu_{asym}(CO_2)$ and $\nu_{sym}(CO_2)$ (293–312 cm^{-1} in **2**, compared to 122–174 cm^{-1} in **1**), indicate significant inequivalence of the carboxylate oxygen atoms, attributed to monodentate coordination mode in **2**, as confirmed by SCXRD studies (*vide infra*).

SCXRD analysis revealed that the molecular structure of **2** is monomeric and features a single *naphtha* ligand bridging two four-coordinate {Me_2Ga(*Me-py*)} units (Fig. 3c). Importantly, no interaction with a fifth donor site is observed, indicating that the gallium centres do not engage in the formation of five-coordinate species. Each Ga center forms a single Ga–O bond (1.910(5) and 1.919(5) Å) to one oxygen atom of the carboxylate group, while the distances to the second oxygen atom (3.045(5) and 3.059(4) Å) are rather long, indicating the absence of any meaningful interaction at the putative fifth coordination site. This observation is consistent with the CShM analysis performed for four- and five-coordinate environments, which indicates a distorted tetrahedral geometry around both Ga centers (see, SI). The two Ga centers are positioned on opposite sides of the naphthalene plane, causing the carboxylate groups to twist out of the aromatic backbone by approximately 30–40° in the same direction (Fig. 3c). The C–O bond lengths within the carboxylate groups fall into two distinct ranges: 1.300(8)–1.303(8) Å for the coordinating O atoms and 1.229(8)–1.231(8) Å for the non-coordinating ones, consistent with localization of the C═O bonds characteristic of a monodentate coordination mode. The coordinated *Me-py* ligands adopt a convergent arrangement relative to the complex, likely stabilized by intramolecular C–H···O hydrogen bonds (H···O distances of 2.402–2.946 Å) (Fig. 3c).

The formation of complex **2** contrasts with our previous studies on the organoaluminum analogue of complex **1**.[16] In that case, the addition of *Me-py* initially induced cleavage of the macrocyclic structure of the parent compound (Fig. 2b). The resulting monomeric [$(Me_2Al)_2$(*naphtha*)(*Me-py*)$_2$] adduct was stable in solution; however, upon crystallization, it underwent reorganization to regenerate the original macrocyclic scaffold, yielding a five-coordinate Lewis acid–base adduct [{$(Me_2Al)_2$(*naphtha*)}$_2$(*Me-py*)$_2$] composed of the parent macrocycle [$(Me_2Al)_2$(*naphtha*)]$_2$ and two coordinated *Me-py* molecules. In contrast, no such transformation is observed for the organogallium complex **1**: the Lewis acid–base adduct **2** retains its monomeric structure in the solid state (Fig. 2f) highlighting the reduced propensity of Ga to exhibit dormant Lewis acidity.

Reactivity of 1 toward various bipyridine linkers

After establishing that **1** can form stable Lewis acid–base adducts with neutral N-donor bases, we next turned our attention to bipyridine ligands as *N*,*N*′-ditopic linkers with the aim of constructing new 1D coordination-driven architectures. Our previous studies demonstrated that, in the case of the organoaluminum complex [$(Me_2Al)_2$(*naphtha*)]$_2$, the nature of the backbone connecting the pyridyl units was crucial for the structure of the resulting adducts (Fig. 2c and d).[16] In particular, the conformationally flexible alkane linker in *bpea* promoted cleavage of the parent tetranuclear complex, affording the macrocyclic complex [$(Me_2Al)_2$(*naphtha*)(*bpea*)]$_2$. In contrast, the more rigid *bpee* linker preserves the core structure of the parent aluminium complex, allowing its incorporation as a node in a 1D coordination polymer [{$(Me_2Al)_2$(*naphtha*)}$_2$(*bpee*)]$_n$. Guided by these findings, we initially examined the reactivity of **1** with *bpea* and *bpee*. Notably, the addition of 2 equivalents of either ligand to **1** led to the formation of isostructural macrocyclic complexes [$(Me_2Ga)_2$(*naphtha*)(*bpea*)]$_2$ (**3**) and [$(Me_2Ga)_2$(*naphtha*)(*bpee*)]$_2$ (**4**) (Fig. 2h and i). High-quality crystals of both compounds were obtained by allowing the post-reaction solutions to stand at room temperature for several hours. The resulting compounds were insoluble in common organic solvents (DCM, THF, toluene), which precluded their characterization by solution NMR spectroscopy.

SCXRD analysis revealed that both compounds possess analogous molecular structures, closely related to the previously described organoaluminum complex [$(Me_2Al)_2$(*naphtha*)(*bpea*)]$_2$.[16] Their molecular frameworks consist of two dinuclear [$(Me_2Ga)_2$(*naphtha*)] units linked by the respective bipyridine ligands, forming a central 36-membered macrocyclic ring (Fig. 4a and b). The organic backbones of the *N*,*N*′-ditopic linkers in both complexes display similar geometries, adopting *anti*- and *trans*-conformations for *bpea* and *bpee*, respectively. All Ga centers exhibit distorted tetrahedral coordination geometries defined by one monodentate carboxylate, one pyridine ligand, and two methyl groups (for CShM analysis, see SI). The carboxylate groups display highly unsymmetrical η^1-coordination, with C–O bond lengths of 1.291(2)–1.294(3) Å for the coordinating oxygen atoms and 1.224(3)–1.231(2) Å for the non-coordinating ones. In both complexes, the two carboxylate groups within each *naphtha* ligand are tilted in the same direction relative to the aromatic plane by *ca.* 30° and 60°. This monodentate coordination mode is likely reinforced by intra- and intermolecular non-covalent C–H···O interactions, with O···H distances in the range of 2.204–2.599 Å. Notably, while in complex **3** only the pyridyl protons can act as hydrogen-bond donors, in **4** the protons of the ethylene backbone may also participate in hydrogen bonding, which likely influences

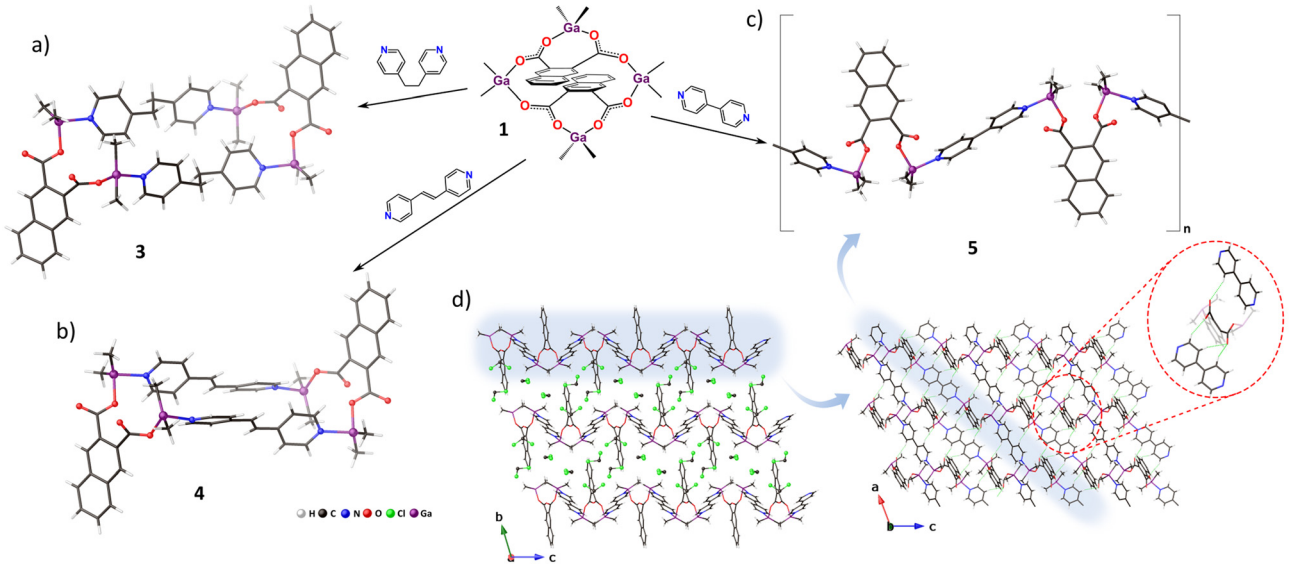

Fig. 4 Reactivity of **1** toward various bipyridine linkers: molecular structures of macrocyclic Lewis acid–base adducts **3** (a) and **4** (b) and molecular structure (c) and self-assembly (d) of 1D coordination polymer **5**.

the crystal packing of molecules. Indeed, although both complexes adopt densely packed crystal structures, the arrangement of molecules differs considerably between **3** and **4** (Fig. S7). The FTIR spectra of complexes **3** and **4** display $\nu_{sym}(CO_2)$ and $\nu_{asym}(CO_2)$ bands at 1614–1644 cm^{-1} and 1340 cm^{-1}, respectively, which are similar to those observed for **2**, in line with a comparable monodentate coordination mode of the carboxylate groups.

The formation of macrocyclic four-coordinate structures by the Lewis adducts of **1** with both *bpea* and *bpee* contrasts with the behavior of the organoaluminum analogues[16] and is consistent with the observed absence of dormant Lewis acidity in the organogallium complex (*vide supra*). Thus, in a further effort to construct a coordination polymer architecture based on Ga building units, we focused on the shorter and more rigid 4,4′-bipyridine (*bipy*) linker, aiming to prevent stabilization of macrocyclic structures. Indeed, the addition of 2 equiv. of *bipy* to DCM solution of **1** led to the spontaneous formation of white crystals of the polymeric Lewis acid–base adduct $[(Me_2Ga)_2(naphtha)(bipy)]_n$ (**5**) (Fig. 4c). The resulting compound was insoluble in common organic solvents (DCM, THF, toluene), which precluded its characterization by solution NMR spectroscopy.

SCXRD analysis revealed that **5** crystallizes as a linear zigzag coordination polymer composed of alternating $[(Me_2Ga)_2(naphtha)]$ moieties linked by linear *N*,*N*′-ditopic *bipy* ligands. The monomeric units of **5** adopt a structure similar to that observed in **2**; however, unlike **2**, the pyridine ligands are oriented divergently (projecting outward from the molecule), facilitating extension of the 1D polymeric structure (Fig. 4c). The individual chains of **5** further self-assemble into 2D supramolecular layers *via* intermolecular C–H···O hydrogen bonds between the carboxylate oxygen atoms and the hydrogen atoms of the pyridine rings (Fig. 4d). In the solid state, these 2D supramolecular layers pack into the crystal structure of **5**, encapsulating DCM molecules within the interlayer spaces. The stoichiometry of the resulting solvates was estimated from elemental analysis as **5**·3.2DCM, though it may vary between samples. Unfortunately, due to the poor quality of the crystals and disorder of the DCM molecules, a fully satisfactory refinement of the crystal structure of **5** could not be achieved (final R = 17.92%), precluding a detailed discussion of geometrical parameters. Nevertheless, the data are sufficient to confirm the general structure of the complex. The FTIR spectrum of **5** displays $\nu_{sym}(CO_2)$ and $\nu_{asym}(CO_2)$ bands at 1642 and 1614 cm^{-1} and 1340 cm^{-1}, respectively, consistent with a monodentate coordination mode of the carboxylate groups.

Reaction of 1 with a chiral *N*,*N*′-ditopic organoaluminium metaloligand

During our previous studies, we demonstrated that alkylaluminum derivatives of chiral cinchonine (CN–H) are highly promising building units for the construction of non-covalent[24,37] and coordination-driven[24,38] homochiral frameworks. In CN-stabilized organoaluminum complexes, cinchonine anions act as O,N-bidentate ligands by engaging their alkoxide and tertiary amine donor sites, whereas the quinoline nitrogen atoms remain uncoordinated. Thus, the resulting complexes can be further exploited as *N*,*N*′-ditopic metalloligands to propagate supramolecular coordination networks *via* dative interactions with Lewis acids. This strategy proved highly successful with simple Zn-based Lewis acids such as $ZnCl_2$ or ZnR_2 (R = Me, Et), yielding new homochiral supramolecular architectures.[24,38] Previously, we also attempted to extend this strategy for more complex dormant poly-Lewis acids, like organoaluminum complex $[(Me_2Al)_2(naphtha)]_2$. However, model reaction with

$[Me_2Al(CN)]_2$ resulted only in the recovery of a mixture of the parent complexes (Fig. 2e).[16] Here, we undertook an analogous approach using the organogallium complex **1**. Remarkably, instead of a simple coordination adduct, the reaction proceeds *via* an unprecedented transalkylation pathway, leading to the formation of a novel heterometallic complex. The reaction of **1** with $[Me_2Al(CN)]_2$ in a 1 : 2 molar ratio in CH_2Cl_2 afforded a new heterometallic Al/Ga complex $[(MeAl)_2(naphtha)(CN)_2(GaMe_3)_2]$ (**6**) (Fig. 5a).

High-quality crystals of **6**·2.25MePh were obtained after recrystallization from the toluene solution at 5 °C. SCXRD analysis revealed that the molecular structure of **6** resembles that of the parent cinchonine-derived complex $[Me_2Al(CN)]_2$, with two Al–Me groups replaced by a bridging *naphtha* ligand, and two $GaMe_3$ molecules coordinated to the quinoline nitrogen atoms of the CN ligands (Fig. 5). The coordination mode of the *naphtha* ligand is similar to that observed in the organogallium complex **2**, with both monodentate carboxylate groups twisted out of the aromatic backbone plane by approximately 33–60° in the same direction. The C–O bonds within the carboxylate groups are highly asymmetric, with lengths of 1.27(2)–1.34(2) Å for the coordinating oxygen atoms and 1.19(2)–1.24 (2) Å for the non-coordinating ones. The Al centers adopt a distorted trigonal–bipyramidal coordination geometry, with the alkoxide oxygen atoms and tertiary amine donors of two different CN ligands occupying the axial positions (for CShM analysis, see SI). The Ga centers exhibit a distorted tetrahedral C_3N coordination environment, and the Ga–N bond lengths (2.140(10)–2.151(12) Å) are comparable to those reported for other pyridine-type Lewis adducts of $GaMe_3$ (2.143(2)–2.152(3) Å).[39,40] Complex **6** crystallizes form toluene a **6**·2.25MePh solvate in the triclinic space group *P*1 with four complex molecules in the asymmetric unit. The solid state FTIR spectrum of **6** shows $\nu_{asym}(CO_2)$ bands at 1660 and 1591 cm^{-1} and $\nu_{sym}(CO_2)$ band at 1455 cm^{-1}, which are similar to those observed for **2**, consisting with a comparable monodentate coordination mode of the carboxylate groups. The ^1H NMR spectrum of **6** in $CDCl_3$ displays sets of resonances characteristic of $naphtha^{2-}$ and CN^- anions, indicating their 1 : 2 molar ratio (Fig. S10). Furthermore, two singlets observed at −0.23 and −1.03 ppm correspond to six Ga–Me and two Al–Me groups, respectively. The ^{13}C NMR spectrum of **6** shows sets of signals associated with carbonyl (172.8 ppm), aromatic (151.6–115.9 ppm), and aliphatic (69.3–22.8 ppm) carbon atoms of *naphtha* and CN ligands, as well as two resonances at −3.3, and −10.7 ppm corresponding to Ga- and Al-bonded methyl groups, respectively.

The isolation of complex **6** from the reaction of **1** with $[Me_2Al(CN)]_2$ highlights the dynamic nature of both coordination systems, revealing unprecedented ligand scrambling involving aluminum-to-gallium alkyl transfer accompanied by reverse gallium-to-aluminum carboxylate migration (Fig. 5a). Notably, we have observed similar reactivity pattern in other reaction system involving CN-based metalloligand, *i.e.* transmetalation between $[MeAl(CN)_2]$ and $ZnEt_2$, leading to the formation of an unusual heterometallic coordination polymer, $[\{(CN)EtAl(\mu\text{-}CN)_2ZnEt\}ZnMe_2]_n$.[38] Notably, in contrast to previously reported transmetalation processes involving low-valent aluminium species,[41] the transformation observed here occurs in a system based on octet-compliant Group 13 centres. Understanding transalkylation and transmetalation phenomena in organometallic systems is crucial for the rational development of heterometallic materials that exploit synergistic interactions between different metal centers, enabling emergent reactivity and fine-tuning of physicochemical properties.[42] For example, transmetalation involving organoaluminum compounds constitutes a key step in the activation of Ziegler–Natta catalysts.[43] However, to the best of our knowledge, transalkylation processes between aluminum and gallium organometallic species remain largely unexplored. In contrast to our findings, Thomas *et al.* reported an opposite direction of alkyl transfer in related systems, demonstrating that heterometallic Group 13/15 adducts of the type $[(DMAP)AlMe_2\text{-}E(SiMe_3)_2]$ (E = P, Sb) react with $GaMe_3$ *via* gallium-to-aluminum methyl transfer, ultimately leading to the elimination of $(DMAP)AlMe_3$.[44] Together, these findings expose a fundamental gap in our understanding of the factors governing alkyl group affinity and transfer between aluminum and gallium centers. Therefore, although the potential of complex **6** for constructing extended coordination polymers is limited –

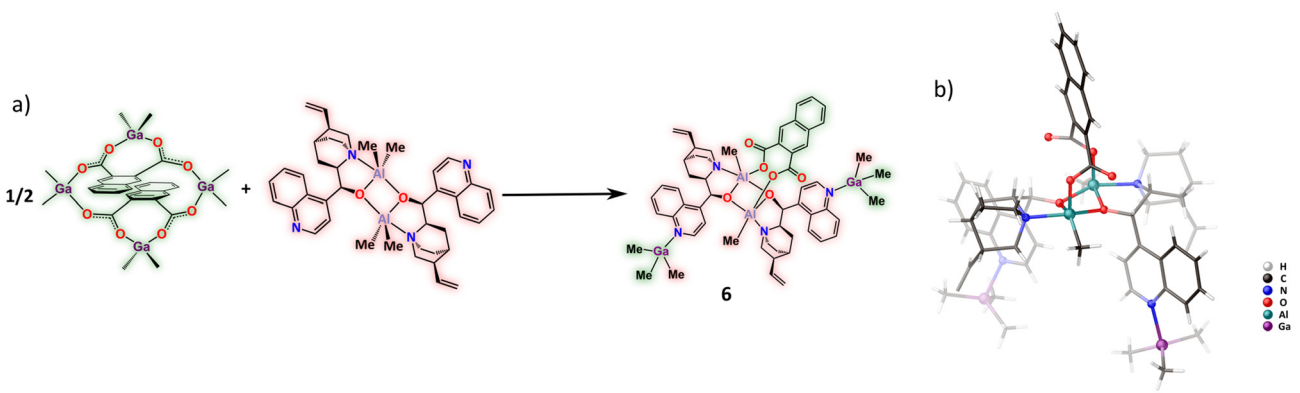

Fig. 5 Schematic representation of the formation of heterometallic complex **6** (a) and its molecular structure (b).

due to the terminal nature of the coordinated $GaMe_3$ units – its structural characterization reveals a promising and previously underexplored facet of Group 13 reactivity that warrants further investigation.

Conclusions

In conclusion, we have investigated the reactivity of a macrocyclic organogallium complex $[(Me_2Ga)_2(naphtha)]_2$ (**1**) toward mono- and bifunctional pyridine Lewis bases as well as the chiral *N*,*N*′-metalloligand $[Me_2Al(CN)]_2$, and compared its behaviour with that of the corresponding organoaluminium analogue, $[(Me_2Al)_2(naphtha)]_2$. The results demonstrate that the nature of the Group 13 metal centre plays a decisive role in governing Lewis acidity and structural outcomes. In contrast to aluminium, the gallium system exhibits a markedly reduced tendency to form five-coordinate species associated with dormant Lewis acidity. Instead, coordination of neutral Lewis bases promotes cleavage of the parent macrocyclic framework and leads to well-defined four-coordinate complexes. Furthermore, the reaction of **1** with the chiral *N*,*N*-ditopic organoaluminium metalloligand reveals an unexpected transalkylation pathway, affording a heterometallic complex through aluminium-to-gallium alkyl transfer and reverse carboxylate migration. This behaviour should be explicitly considered in the rational design of heterometallic materials but also provides opportunities for generating emergent structures through controlled metal exchange processes.

From a design perspective, these findings indicate that the choice of the Group 13 metal centre can serve as a key parameter for controlling the balance between structural stability and reactivity in coordination-driven assembly. In particular, the reduced propensity of gallium to adopt higher coordination numbers favours the predictable formation of discrete or polymeric architectures based on four-coordinate nodes, whereas aluminium systems introduce additional flexibility associated with dormant Lewis acidity. Overall, these findings provide new insight into the relationship between metal identity, coordination preferences, and reactivity in Group 13 organometallic chemistry, offering guidelines for the rational design of coordination architectures based on main-group building blocks.

Experimental section

General remarks

All manipulations were conducted under a nitrogen atmosphere by using the standard Schlenk technique. All reagents were purchased from commercial vendors and used as received. $[Me_2Al(CN)]_2$ was prepared was prepared according to the previously described procedure.[24] **Caution!** Because of the pyrophoric nature of $AlMe_3$ and $GaMe_3$ special caution should be adopted. Solvents were purified and dried using MBraun Solvent Purification System (SPS). NMR spectra were recorded on a JEOL JNM-ECZL (600 MHz) spectrometer. FTIR spectra were recorded on a Bruker-Tensor II (ATR) spectrometer. Elemental analyses were performed on the Elementar VarioMicro Cube analyzer.

Synthesis of 1

A solution of $GaMe_3$ in hexane (1 M, 1 mL, 1 mmol) was added to a solution of *naphtha*-H_2 (0.108 g, 0.5 mmol) in DCM (5 mL) at −78 °C. The reaction mixture was stirred at room temperature overnight. Single crystals of **1**·0.5DCM for SCXRD analysis were obtained from the concentrated parent solution by crystallization at 5 °C (0.370 g, 85%). Alternatively, the solvent can be removed under vacuum to give the product as a white crystalline powder in a practically quantitative yield. ^{1}H NMR ($CDCl_3$, 600 MHz): δ = 8.43 (s, 4H, Ar), 8.00 (m, 4H, Ar), 7.68 (m, 4H, Ar), −0.03 (s, 12H, Ga–Me), −0.66 (s, 6H, Ga–Me), −0.84 (s, 6H, Ga–Me); ^{13}C NMR ($CDCl_3$, 150 MHz): δ = 177.6, 133.7, 132.4, 129.2, 129.0, 128.9, −5.8, −7.6, −8.1; FTIR (ATR, cm^{-1}): $\tilde{\nu}$ [cm^{-1}] = 3062 (w), 2966 (w), 1589 (m), 1537 (s), 1498 (m), 1470 (m), 1447 (m), 1415 (s), 1353 (w), 1200 (w), 882 (w), 765 (m), 735 (s), 705 (m), 601 (s), 547 (s), 477 (m). Elemental analysis (%) calcd for **1**·0.47DCM $C_{32.47}H_{36.94}O_8Cl_{0.94}Ga_4$: C 44.96, H 4.29; found: C 44.97, H 4.31.

Synthesis of 2

Me-py (0.093 g, 1 mmol) was added to a solution of **1** (0.207 g, 0.25 mmol) in DCM (5 ml). The solution was concentrated, and colorless crystals of **2** were obtained upon crystallization at 5 °C (0.200 g, 67%). ^{1}H NMR ($CDCl_3$, 600 MHz): δ = 8.52 (d, J = 4.8 Hz, 4H, Ar^{py}), 8.16 (s, 2H, $Ar^{naphtha}$), 7.83 (m, 2H, $Ar^{naphtha}$), 7.47 (m, 2H, $Ar^{naphtha}$), 7.29 (d, J = 5.2 Hz, 4H, Ar^{py}), 2.41 (s, 6H, Me^{py}), −0.17 (s, 12H, Ga–Me); ^{13}C NMR ($CDCl_3$, 150 MHz): δ = 174.3, 151.7, 147.5, 134.0, 133.3, 128.7, 128.4, 127.0, 126.1, 21.5, −6.5; FTIR (ATR, cm^{-1}): $\tilde{\nu}$ [cm^{-1}] = 3053 (w), 2961 (w), 1640 (s), 1621 (s), 1501 (w), 1447 (w), 1357 (w), 1330 (s), 1328 (s), 1205 (w), 1194 (w), 1035 (m), 809 (s), 769 (m), 726 (m), 703 (m), 586 (s), 539 (m), 485 (s), 479 (s). Elemental analysis (%) calcd for **2** $C_{28}H_{32}N_2O_4Ga_2$: C 56.05, H 5.38, N 4.67; found: C 56.00, H 5.31, N 4.70.

Synthesis of 3

bpea (0.092 g, 0.5 mmol) was added to a solution of **1** (0.207 g, 0.25 mmol) in DCM (5 ml). After a few minutes, colorless square-shaped crystals of **3** were formed (0.275 g, 92%). The product was insoluble in common organic solvents (DCM, THF, toluene). FTIR (ATR, cm^{-1}): $\tilde{\nu}$ [cm^{-1}] = 3073 (w), 2959 (w), 1644 (m), 1615 (s), 1466 (w), 1432 (w), 1365 (m), 1340 (s), 1310 (m), 1208 (w), 1193 (w), 1068 (w), 1031 (m), 832 (w), 815 (m), 767 (w), 745 (m), 731 (m), 588 (s), 540 (s), 475 (m), 454 (m). Elemental analysis (%) calcd for **3** $C_{56}H_{60}N_4O_8Ga_4$: C 56.24, H 5.06, N 4.68; found: C 56.10, H 5.07, N 4.75.

Synthesis of 4

bpee (0.090 g, 0.5 mmol) was added to a solution of **1** (0.207 g, 0.25 mmol) in DCM (5 ml). After a few minutes, colorless square-shaped crystals of **4** were formed (0.265 g, 89%). The

product was insoluble in common organic solvents (DCM, THF, toluene). FTIR (ATR, cm^{-1}): $\tilde{\nu}$ [cm^{-1}] = 3101 (w), 2958 (w), 1642 (s), 1614 (s), 1464 (w), 1435 (w), 1369 (m), 1340 (s), 1308 (w), 1204 (w), 1032 (m), 836 (m), 810(m), 748 (m), 729 (m), 591 (s), 569 (m), 551 (s), 479 (m), 455 (m). Elemental analysis (%) calcd for **4** $C_{56}H_{56}N_4O_8Ga_4$: C 56.43, H 4.74, N 4.70; found: C 56.32, H 4.63, N 4.78.

Synthesis of 5

bipy (0.078 g, 0.5 mmol) was added to a solution of **1** (0.207 g, 0.25 mmol) in DCM (5 ml). After a few minutes, colorless regular crystals of **5**·xDCM were formed (0.285 g). The product was insoluble in common organic solvents (DCM, THF, toluene). FTIR (ATR, cm^{-1}): $\tilde{\nu}$ [cm^{-1}] = 3105 (w), 2957 (w), 1641 (s), 1612 (s), 1460 (w), 1417 (w), 1370 (w), 1340 (m), 1333 (s), 1300 (m), 1208 (w), 1078 (w), 810 (w), 807 (m), 732 (m), 645 (s), 587 (s), 540 (m), 470 (m). Elemental analysis (%) calcd for **5**·3.2DCM $C_{31.2}H_{36.4}N_2O_4Cl_{6.4}Ga_2$: C 43.09, H 4.22, N 3.22; found: C 43.08, H 4.37, N 3.26.

Synthesis of 6

A solution of **1** (0.207 g, 0.25 mmol) in DCM (3 ml) was added to a solution of $[Me_2Al(CN)]_2$ (0.078 g, 0.5 mmol) in DCM (3 ml), and the resulting mixture was stirred overnight at room temperature. Small colorless crystals of **6** were isolated by crystallization from the concentrated reaction mixture upon addition of hexane (0.200 g, 70%). SCXRD-quality monocrystals of **6**·2.25MePh were obtained by recrystallization of the crude product from toluene at 5 °C. ^{1}H NMR ($CDCl_3$, 600 MHz): δ = 9.16 (d, J = 4.9 Hz, 2H, Ar^{CN}), 8.60 (d, J = 8.6 Hz, 2H, Ar^{CN}), 8.33 (s, 2H, $Ar^{naphtha}$), 8.09 (d, J = 8.6 Hz, 2H, Ar^{CN}), 7.97 (m, 2H, $Ar^{naphtha}$), 7.88 (d, J = 4.9 Hz, 2H, Ar^{CN}), 7.86 (m, 2H, Ar^{CN}), 7.70 (m, 2H, Ar^{CN}), 7.62 (m, 2H, $Ar^{naphtha}$), 6.98 (d, J = 8.4 Hz, 2H, OCH), 4.62 (ddd, J = 16.8, 10.5, 6.3 Hz, 2H, =C(R)H), 4.55 (dd, J = 10.5, 1.3 Hz, 2H, $=CH_2$), 4.32 (dd, J = 16.8, 1.3 Hz, 2H, $=CH_2$), 3.83 (m, 2H, quinuclidine-H), 3.23 (m, 2H, quinuclidine-H), 2.82 (m, 2H, quinuclidine-H), 2.57 (m, 4H, quinuclidine-H), 0.8–2.1 (m, 12H, quinuclidine-H), −0.23 (s, 18H, Ga–Me), −1.03 (s, 6H, Al–Me); ^{13}C NMR ($CDCl_3$, 150 MHz): δ = 172.8, 151.6, 149.1, 145.4, 136.9, 134.2, 133.5, 130.8, 130.3, 128.7, 128.0, 127.9, 124.3, 119.4, 115.9, 69.3, 69.2, 68.5, 48.2, 38.1, 27.3, 26.6, 24.6, 22.8, −3.3, −10.7; FTIR (ATR, cm^{-1}): $\tilde{\nu}$ [cm^{-1}] = 3070 (w), 2925 (s), 2872 (m), 1660 (s), 1591 (s), 1567 (s), 1513 (m), 1455 (s), 1417 (m), 1386 (m), 1362 (m), 1332 (s), 1300 (m), 1202 (w), 1092 (w), 1058 (w), 994 (w), 895 (w), 848 (w), 805 (m), 768 (s), 705 (m), 661 (s), 602 (m), 540 (m), 477 (m), 417 (w). Elemental analysis (%) calcd for **6**·1.1DCM $C_{59.1}H_{74.2}N_4O_6Cl_{2.2}Al_2Ga_2$: C 58.76, H 6.19, N 4.64; found: C 58.83, H 6.69, N 4.32.

X-Ray structure determination

The crystals were selected under Paratone-N oil, mounted on the nylon loops, and positioned in the cold stream on the diffractometer. The X-ray data for complexes **1**, **3**, **4**, and **5**, were collected at 100(2) K on a SuperNova Agilent diffractometer using graphite monochromated MoKα radiation (λ = 0.71073 Å). The data was processed with CrysAlisPro.[45] The X-ray data for **2** was collected at 100(2) K on a Nonius Kappa CCD diffractometer using graphite monochromated MoKα radiation (λ = 0.71073 Å), using diffractometer control program "Collect".[46] The crystal structures were solved by direct methods using the SHELXS-97[47] program and were refined by full-matrix least-squares on F^2 using the program SHELXL-program[48] implemented in the Olex2[49] suite. All non-hydrogen atoms were refined with anisotropic displacement parameters. Hydrogen atoms were added to the structure model at geometrically idealized coordinates and refined as riding atoms. CCDC: 2530613 (**1**), 2530619 (**2**), 2530614 (**3**), 2530615 (**4**), 2530616 (**5**), 2530618 (**6**).

The coordination sphere geometries of metal centers in the presented structures were analyzed employing the continuous shape measurement (CShM)[50] using SHAPE software.[51] The results are presented in Table S12 in SI.

Conflicts of interest

There are no conflicts to declare.

Data availability

The other data supporting this article have been included as part of the supplementary information (SI). Supplementary information: X-Ray crystallography data, CShM analysis, NMR and FTIR spectra. See DOI: https://doi.org/10.1039/d6dt00374e.

CCDC 2530613 (**1**), 2530614 (**3**), 2530615 (**4**), 2530616 (**5**), 2530618 (**6**) and 2530619 (**2**) contain the supplementary crystallographic data for this paper.[52a–f]

Acknowledgements

The authors acknowledge the financial support of the National Science Centre, Poland (Grant OPUS 19, No. 2020/37/B/ST4/03310).

References

1 C. Janiak, *J. Chem. Soc., Dalton Trans.*, 2003, **3**, 2781–2804.
2 S. Kitagawa, R. Kitaura and S. Noro, *Angew. Chem., Int. Ed.*, 2004, **43**, 2334–2375.
3 W. L. Leong and J. J. Vittal, *Chem. Rev.*, 2011, **111**, 688–764.
4 H. Furukawa, K. E. Cordova, M. O'Keeffe and O. M. Yaghi, *Science*, 2013, **341**, 1230444.
5 J. Zhao, J. Yuan, Z. Fang, S. Huang, Z. Chen, F. Qiu, C. Lu, J. Zhu and X. Zhuang, *Coord. Chem. Rev.*, 2022, **471**, 214735.
6 L. M. Aguirre-Díaz, D. Reinares-Fisac, M. Iglesias, E. Gutiérrez-Puebla, F. Gándara, N. Snejko and M. Á. Monge, *Coord. Chem. Rev.*, 2017, **335**, 1–27.

7 S. Mukherjee, A. V. Desai and S. K. Ghosh, *Coord. Chem. Rev.*, 2018, **367**, 82–126.
8 D. Wu, P. F. Zhang, G. P. Yang, L. Hou, W. Y. Zhang, Y. F. Han, P. Liu and Y. Y. Wang, *Coord. Chem. Rev.*, 2021, **434**, 213709.
9 S. Li, Y. Chen, X. Pei, S. Zhang, X. Feng, J. Zhou and B. Wang, *Chin. J. Chem.*, 2016, **34**, 175–185.
10 U. T. Uthappa, K. V. Ajeya, V. Sannasi, S. G. Lee, E.-H. Sohn, B.-J. Chang, I.-J. Park, J. H. Kim, M. D. Kurkuri and H.-Y. Jung, *J. Water Process Eng.*, 2024, **63**, 105450.
11 N. Y. Gugin, A. Virovets, E. Peresypkina, E. I. Davydova and A. Y. Timoshkin, *CrystEngComm*, 2020, **22**, 4531–4543.
12 T. C. Schäfer, J. Becker, M. T. Seuffert, D. Heuler, A. E. Edykh and K. Müller-Buschbaum, *Chem. – Eur. J.*, 2022, **28**, e202104171.
13 J. Lewiński and A. E. H. Wheatley, in *Top Organomet Chem*, 2012, vol. 48, pp. 1–58.
14 A. Y. Timoshkin, *Chem. – Eur. J.*, 2024, **30**, e202302457.
15 T. Schäfer and K. Müller-Buschbaum, *Z. Anorg. Allg. Chem.*, 2018, **644**, 1791–1795.
16 M. Terlecki, I. Justyniak, D. Prochowicz and J. Lewiński, *Eur. J. Inorg. Chem.*, 2020, 119–127.
17 N. Y. Gugin, A. V. Virovets, E. Peresypkina, E. I. Davydova and A. Y. Timoshkin, *CrystEngComm*, 2022, **24**, 8266–8278.
18 A. Y. Robin and K. M. Fromm, *Coord. Chem. Rev.*, 2006, **250**, 2127–2157.
19 V. C. Gibson, C. Redshaw, A. J. P. White and D. J. Williams, *Angew. Chem., Int. Ed.*, 1999, **38**, 961–964.
20 W. Uhl, A.-C. Fick, T. Spies, G. Geiseler and K. Harms, *Organometallics*, 2004, **23**, 72–75.
21 C. Redshaw, M. R. J. Elsegood and K. E. Holmes, *Angew. Chem., Int. Ed.*, 2005, **44**, 1850–1853.
22 J. Lewiński, W. Bury, I. Justyniak and J. Lipkowski, *Angew. Chem., Int. Ed.*, 2006, **45**, 2872–2875.
23 I. Justyniak, W. Bury, D. Prochowicz, K. Wójcik, J. Zachara and J. Lewiński, *Inorg. Chem.*, 2014, **53**, 7270–7275.
24 T. Kaczorowski, I. Justyniak, T. Lipińska, J. Lipkowski and J. Lewiński, *J. Am. Chem. Soc.*, 2009, **131**, 5393–5395.
25 C. E. Bethley, C. L. Aitken, C. J. Harlan, Y. Koide, S. G. Bott and A. R. Barron, *Organometallics*, 1997, **16**, 329–341.
26 D. A. Dickie, D. D. Choytun, M. C. Jennings, H. A. Jenkins and J. A. Clyburne, *J. Organomet. Chem.*, 2004, **689**, 2186–2191.
27 W. Ziemkowska, M. Cyrański and A. Kunicki, *Inorg. Chem.*, 2009, **48**, 7006–7008.
28 L. Kalita, R. Pothiraja, V. Saraf, M. G. Walawalkar, R. J. Butcher and R. Murugavel, *J. Organomet. Chem.*, 2011, **696**, 3155–3161.
29 I. Justyniak, D. Prochowicz, A. Tulewicz, W. Bury, P. Goś and J. Lewiński, *Dalton Trans.*, 2017, **46**, 669–677.
30 C. Bour and V. Gandon, *Coord. Chem. Rev.*, 2014, **279**, 43–57.
31 S. Dagorne and R. Wehmschulte, *ChemCatChem*, 2018, **10**, 2509–2520.
32 C. Redshaw and M. R. J. Elsegood, *Chem. Commun.*, 2001, 2016–2017.
33 M. K. Pal, N. P. Kushwah, A. P. Wadawale, V. S. Sagoria, V. K. Jain and E. R. T. Tiekink, *J. Organomet. Chem.*, 2007, **692**, 4237–4243.
34 M. R. Kaluđerović, S. Gómez-Ruiz, B. Gallego, E. Hey-Hawkins, R. Paschke and G. N. Kaluđerović, *Eur. J. Med. Chem.*, 2010, **45**, 519–525.
35 S. Gómez-Ruiz, J. Ceballos-Torres, S. Prashar, M. Fajardo, Ž. Žižak, Z. D. Juranić and G. N. Kaluđerović, *J. Organomet. Chem.*, 2011, **696**, 3206–3213.
36 E. Jaśkowska, D. Basiak, Ł. Dobrzycki, P. Rzepiński, P. Socha, C. Cadar, I. Justyniak, T. Wojciechowski and W. Ziemkowska, *J. Organomet. Chem.*, 2016, **819**, 228–236.
37 J. Lewiński, T. Kaczorowski, D. Prochowicz, T. Lipińska, I. Justyniak, Z. Kaszkur and J. Lipkowski, *Angew. Chem., Int. Ed.*, 2010, **49**, 7035–7039.
38 T. Kaczorowski, I. Justyniak, D. Prochowicz, K. Zelga, A. Kornowicz and J. Lewiński, *Chem. – Eur. J.*, 2012, **18**, 13460–13465.
39 H.-S. Sun, X.-M. Wang, X.-Z. You and X.-Y. Huang, *Polyhedron*, 1995, **14**, 2159–2163.
40 B. J. Hellmann, A. Mix, B. Neumann, H.-G. Stammler and N. W. Mitzel, *Dalton Trans.*, 2010, **39**, 7073–7079.
41 E. Hevia and F. Dankert, *Eur. J. Inorg. Chem.*, 2024, **27**, e202400418.
42 J. Campos, *Nat. Rev. Chem.*, 2020, **4**, 696–702.
43 D. V. Stukalov and V. A. Zakharov, *J. Phys. Chem. C*, 2009, **113**, 21376–21382.
44 F. Thomas, S. Schulz, H. Mansikkamäki and M. Nieger, *Organometallics*, 2003, **22**, 3471–3477.
45 CrysAlisPro, *Data Collection and Processing Software for Agilent X-ray Diffractometers, ver. 1.171.35.21b*, Agilent Technologies, 2012.
46 B. V. Nonius, *"Collect" data collection software*, 1998.
47 G. M. Sheldrick, *Acta Crystallogr., Sect. A:Found. Crystallogr.*, 1990, **46**, 467–473.
48 G. M. Sheldrick, *SHELX-97 (Program for the Refinement of Crystal Structures)*, University of Göttingen, Germany, 1997.
49 O. V. Dolomanov, L. J. Bourhis, R. J. Gildea, J. A. K. Howard and H. Puschmann, *J. Appl. Crystallogr.*, 2009, **42**, 339–341.
50 H. Zabrodsky, S. Peleg and D. Avnir, *J. Am. Chem. Soc.*, 1992, **114**, 7843–7851.
51 M. Llunell, D. Casanova, J. Cirera, P. Alemany and S. Alvarez, *SHAPE Version 2.1*, 2013.
52 (*a*) CCDC 2530613: Experimental Crystal Structure Determination, 2026, DOI: 10.5517/ccdc.csd.cc2qy9pp; (*b*) CCDC 2530614: Experimental Crystal Structure Determination, 2026, DOI: 10.5517/ccdc.csd.cc2qy9qq; (*c*) CCDC 2530615: Experimental Crystal Structure Determination, 2026, DOI: 10.5517/ccdc.csd.cc2qy9rr; (*d*) CCDC 2530616: Experimental Crystal Structure Determination, 2026, DOI: 10.5517/ccdc.csd.cc2qy9ss; (*e*) CCDC 2530618: Experimental Crystal Structure Determination, 2026, DOI: 10.5517/ccdc.csd.cc2qy9vv; (*f*) CCDC 2530619: Experimental Crystal Structure Determination, 2026, DOI: 10.5517/ccdc.csd.cc2qy9ww.